Journal of Engineering Technology and Applied Physics

Multiphase Flow Pattern Hydrodynamics of Carbon Dioxide and Water in Microchannel Reactor

Muhammad Adam Aiman Amir[1], Mohammad Fahmi Al Alam[1], Afiq Mohd Laziz[1,*] and Jens Denecke[2]
[1]*Department of Chemical Engineering, Universiti Teknologi PETRONAS 32610 Seri Iskandar, Perak, Malaysia.*
[2]*Institute for Thermo-Fluid-Dynamics, Karlsruhe University of Applied Sciences, Karlsruhe 76133, Germany.*
**Corresponding author*: afiq.laziz@utp.edu.my, *ORCiD*: 0000-0003-4905-183X
https://doi.org/10.33093/jetap.2025.7.2.8
Manuscript Received: 9 April 2025, Accepted: 5 June 2025, Published: 15 September 2025

***Abstract*—The utilization of CO_2 is crucial to convert waste into valuable products, such as fuels. Microchannel reactor technology has gained attention for CO_2 utilization due to their higher interfacial area compared to traditional reactors. Understanding flow regimes is critical for optimizing mass transfer efficiency. Hence, this project aims to create a new flow pattern map for CO_2 and water and investigate how gas bubble and liquid slug properties are affected by the change in superficial velocity. Thus, the interfacial area for each flow pattern can be observed which affects the mass transfer performance. The dimensions of flow pattern were measured, so the interfacial area could be calculated accordingly. The amount of CO_2 absorbed into water was determined using the titration method. Then the liquid side mass transfer coefficient for slug flow was determined from the models proposed by van Baten and Krishna (2004). In the end, the rate of mass transfer was determined for slug flow. The results show that slug flow is formed at high gas-to-liquid ratio. Longer slug flow has higher interfacial area and more CO_2 is absorbed through diffusion. A larger interfacial area contributes to higher mass transfer rate, so this proves that the microchannel is good for CO_2 utilization process.**

Keywords*—Circular microchannel, Mass transfer, Flow pattern map, Slug flow, Interfacial area.

I. INTRODUCTION

Global warming and climate change are largely caused by the increasing amount of carbon dioxide (CO_2) in the atmosphere, which causes serious environmental problems. Statistics show that the CO_2 emission trend is increasing every year where Malaysia has produced 288.82 million tonnes of CO_2 from fossil fuels and industry and the whole world produced 37.79 billion tonnes of CO_2 in 2023 [1]. The Carbon Capture, Utilization, and Storage (CCUS) family of technologies intend to absorb carbon dioxide (CO_2) from emissions, keep it out of the atmosphere, and either store or transform them into useful products. The term CO_2 utilization refers to the process of producing valuable products from the waste CO_2. Since CO_2 is a thermodynamically stable molecule, under standard conditions, its conversion into other compounds is energy-intensive and kinetically slow. So, advanced reactor technologies are needed to improve reaction efficiency and selectivity to overcome these challenges.

Microchannel reactor has emerged as a promising solution in the field of CO_2 utilization. In comparison to conventional reactor, this reactor's high surface area-to-volume ratio and micrometer-sized channels greatly increase the heat and mass transfer rate [2]. Microchannel reactors are investigated for CO_2 conversion processes because of their improved transport qualities, which also result in faster reaction kinetics, higher conversion efficiencies, and the capacity to operate under precisely controlled conditions. Within the reactor, the flow pattern influences the efficiency of mixing and mass transfer. Understanding and controlling the flow patterns inside the reactor is therefore essential to optimize microchannel reactors regarding multiphase reactions. The flow pattern slug flow, which is distinguished by alternating liquid and gas slugs, has been found to be very beneficial because of its increased interfacial area and mixing, both of which can enhance the overall performance of mass transfer. This study is important to maximize the usage of microchannel reactor for multiphase reactions. This study focuses on one of the criteria which is to study the mass transfer between two phases based on the interfacial area.

Published by MMU PRESS. URL: https://journals.mmupress.com/index.php/jetap/index

The limitation of conventional reactors regarding the mass transfer rate motivated further studies on microreactors with higher interfacial area for CO_2 utilization. This study aims to develop a flow pattern map for circular microchannel reactors with different superficial velocities of CO_2 and water since there is limitation on flow pattern map involving circular microchannel. In addition, the effect of gas-to-liquid ratio for multiphase flow is not fully understood. Thus, various pairs of CO_2 and water superficial velocities will be used to identify their effect on the flow dimensions, and interfacial area for mass transfer. Most of the current research involving CO_2 are using rectangular microchannel so the application of circular microchannel require specific research for this dimension. There is one flow pattern map from [3] using circular microchannel, but the setup was different where in this research, a T-junction is used. Other experiments using circular microchannel were involving air instead of CO_2 [4], so the flow pattern maps were slightly different. Additionally, this research further analyses on the interfacial area and mass transfer rate accordingly to study the effect of mass transfer area. The detail analysis on mass transfer rate for slug flow is a new study included in this paper.

This project is an experimental project that investigate the CO_2 and water flow regimes inside a 700 µm circular microchannel reactor. This study focuses on a single microchannel for two phases of flow which are CO_2 (gas) and water (liquid). Different inlet superficial velocities specifically 0.07 – 0.15 m/s for CO_2 and 0.009 – 0.035 m/s for water will be used to achieve the first objective. By using different pairs of gas and liquid flow rates, a flow pattern map for CO_2 and water in a circular microchannel can be developed. The second objective of the study is to investigate the impact of gas-to-liquid ratio on the flow pattern dimensions and corresponding interfacial area. The flow inside the microchannel will be measured based on flow visualizations. The variations of the phases' dimensions contribute to the different interfacial area for mass transfer. It is crucial to maximize the interfacial area for a higher mass transfer rate. In addition, for slug flow, the mass transfer rate is evaluated using appropriate correlations.

II. LITERATURE REVIEW

Microreactors are defined by their small-scale channels, which typically range from 1 µm to 1mm in hydraulic diameter and give a high surface area-to-volume ratio, hence increasing the rate of heat and mass transfer [5]. High specific interfacial area improves the reaction kinetics for diffusive processes in the micro- reactors. Additionally, very large gas–liquid interfacial areas up to 20000 m^2/m^3 considerably boost mass transfer rates between the gas and liquid phases [6].

Furthermore, narrow channel diameters reduce diffusion lengths, allowing reactants to travel quickly to reaction sites and thereby decreasing the restrictions associated with mass transport. Due to their larger surface area to volume ratio, microreactors can speed up the reaction rate since they reduce the diffusion rate and enhance mass transfer [7]. Under the same operating conditions, the microreactor's residence time was less than that of the batch reactor. Another fundamental principle is precise control over flow regimes. In microchannel reactors, a variety of flow patterns may be created, including slug flow, which improves mixing and phase contact. Furthermore, microchannel reactors have better heat transmission capabilities, allowing for more precise temperature control during exothermic or endothermic processes. In addition to lowering process costs, decreasing the size of chemical reactors has numerous other advantages, such as less environmental risk and increased safety because of the smaller hold up of hazardous materials [6].

The efficiency of heat and mass transfer, reaction kinetics, and overall reactor performance are all significantly influenced by the flow patterns. To optimize reactor design and operation for diverse chemical processes, it is imperative to comprehend the varieties of flow patterns that are formed in microchannel reactors. Various flow regimes may occur when two immiscible fluids are introduced into a microchannel. Influencing factors are the flow rate of gas and liquid, the characteristics of the fluid, the liquid's wettability on the channel wall, or the dimensions and shape of the channel [8].

The gas and liquid are injected at a co-current flow. The flow inside a microchannel is usually laminar. Few types of flow regimes were found in previous experiments. There are bubbly flow, slug flow, annular flow and stirred flow found in a square 200 µm × 200 µm microchannel which involves CO_2 and methanol-water. Other than that, inside a 3 mm diameter Y-microchannel, slug flow, bubble flow, wall-attached flow, annular flow, and rhombic flow have been observed. Another T-microchannel with a 1.5 mm diameter experienced annular flow, stirring flow and bubble slug circulation. The slug flow, annular flow, bubbly flow, and droplet flow are the four main types of two-phase flow patterns in microchannels as shown in Fig. 1 with their own unique properties that influence the reactor's performance [9].

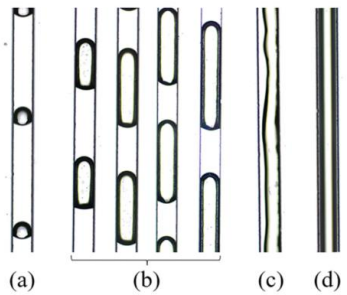

Fig. 1. Flow patterns inside T-microchannel. (a) Bubble flow, (b) Taylor flow, (c) Transition flow and (d) Annular flow.

Bubbly flow describes a regular bubble interval that is formed when the gas phase superficial velocity is substantially lower than the liquid phase superficial

velocity [9]. The bubbles are spherical where the size is smaller than the channel diameter. Despite providing effective mixing, this pattern's mass transfer efficiency is less than in slug flow because of the smaller surface area at gas-liquid interface. Next, the slug flow, or Taylor flow is the most frequently researched due to its mass and heat transfer characteristics. It can be recognized where there are alternates of gas and liquid slugs flowing through the microchannel. This flow is distributed widely and has periodic bubbles with liquid slug spacing. Both gas bubble and liquid slug length exceed the microchannel width. The bubble in Taylor Flow has a seamless body and tail, and a hemisphere-shaped head [9]. Bubbles are also separated from the channel wall by a thin liquid film. This flow pattern is especially helpful for two-phases systems which are gas-liquid and liquid-liquid in microchannel because of continuously refreshing the liquid-gas interface. Additionally, the slug flow regime facilitates excellent mixing inside the liquid slugs, which makes it perfect for gas-liquid reactions and other applications where effective mass transfer is crucial.

For annular flow, there is a total separation between the liquid and gas phases. A thin layer of liquid flows closes to the walls of the channel, and a gas core passes through its center. As the vaporization progresses at moderate vapor quality, the vapor region at the channel's center expands and a liquid layer gradually forms on the channel sides [10]. Higher gas flow rates are experienced in this flow regime, which facilitates effective heat transfer. This is quite helpful in processes where fast heat removal is necessary to preserve reaction stability. Then, the transition flow or stratified flow refers to a transition phase from slug flow to annular flow. There is a well-defined boundary between the gas and liquid phases. It can be observed in conditions of high gas velocity and low liquid velocity [11]. Stratification is maintained because the liquid tends to occupy the bottom part of the channel, and the gas phase flows above it. However, the flow is unique only to non-circular channels, as the film closes in round channels, resulting in an annular flow [11].

For two-phase microchannel, slug flow is the primary flow pattern which is usually present in most of the flow pattern maps for different sizes of microchannel reactors. Slug flow inside a microchannel offers a big advantage on the largest specific surface area [9]. The large interfacial area contributes to a better mass transfer between gas and liquid phases. Plus, the circulation flow inside the liquid slug continuously renews the liquid interface enhancing the mass transfer process [12]. So, the slug flow is the most desired for the two-phases system to ensure the ability of the microchannel can be fully utilized especially on the interfacial area factor. According to the study, when the channel's diameter increased, the slug flow pattern emerged at a lower gas-liquid two-phase flow rate [9]. A specific study on the flow rates or superficial velocities of liquid and gas at fixed microchannel size is required to determine the acceptable range to obtain this slug flow for CO_2. From the current research, the gas-to-liquid ratio is the main factor in the slug flow formation which can be monitored from various flow pattern maps. Furthermore, for Taylor flow, the slug dimension can be varied with different settings such as flow rates or superficial velocities.

There is a relationship between velocity and flow rate from the Eq. (1) where Q is the flow rate, A is the cross-sectional area of the flow, and v is the fluid velocity. The flow rate is directly proportional to the velocity which can be determined with the knowledge of the cross-sectional area of the respective microchannel reactor. Increasing the gas superficial velocity at constant liquid superficial velocity will create longer gas bubbles and shorter liquid slug between the bubbles [3, 12, 13]. The increment in the gas-to-liquid flow rates ratio or superficial velocities leads to longer gas bubbles and shorter liquid slug [9, 12].

$$Q = Av \tag{1}$$

Mass transfer is the movement of mass from one location to another location. It can occur in a single phase or multiphase where it will cross the phase boundaries. The mass transfer rate is a critical factor that significantly influences the performance of chemical reactions in reactors including microchannel reactors. It can be represented by the Eq. (2) where $\dot{m}$ is the mass transfer rate, k_c is the mass transfer coefficient, A is the surface area and ΔC is the concentration gradient. Theoretically, higher mass transfer area contributes to higher mass transfer rate.

$$\dot{m} = k_c \times A \times \Delta C \tag{2}$$

Different fluids may have different mass transfer coefficients. It depends on the solute's diffusivity and the hydrodynamic properties of the phases [14]. So, different reactants require specific information related to the fluids used. However, the mass transfer area factor is applicable for all situations. The general outcomes or trends from the interfacial area effects on mass transfer can be a guideline for CO_2 utilization using microchannels even with different fluids. The interfacial area refers to the total surface area where two different phases come into contact in a controlled volume. The small dimensions of the microchannel reactor provide more surfaces for interaction between gas and liquid for a given volume of the reactants. Hence, it significantly increases the surface area-to-volume ratio. Then, the different types of flow regimes inside the microchannel also lead to different sizes of interfacial area due to different flow pattern dimensions that are formed [15]. To maximize the interfacial area inside a fixed size of microchannels, the liquid and gas flow rates can be manipulated accordingly to achieve the desired flow regimes.

The following mass transfer models for slug flow were proposed by van Baten and Krishna (2004) through Higbie penetration theory [16, 17]. Liquid side mass transfer coefficient, $k_L a$ mostly depends on the liquid slug length. From their experiments, the

mass transfer from the bubble caps to the liquid slug accounted for the majority of the contribution. The correlation can be expressed as Eq. (3) where it shows an increment of $k_L a$ when the bubble velocity increased or liquid slug length reduced. However, it was further developed into Eq. (4) after combining the penetration theory and empirical representations which shows high dependency on the bubble velocity or unit cell length. This expression implies that the thin liquid film also contributes to the mass transfer and is not negligible since the measured $k_L a$ is determined in whole unit cell and not only the liquid slug length.

$$k_L a = \frac{2}{\sqrt{\pi}}\sqrt{\frac{DU_B}{(L_B - d_h)}}\frac{4(L_B - d_h)}{d_h(L_B + L_S)} + 2\frac{\sqrt{2}}{\pi}\sqrt{\frac{DU_B}{d_h}\frac{4}{(L_B + L_S)}} \quad (3)$$

$$k_L a = \frac{2}{d_h}\left(\frac{Du_B}{L_B + L_S}\right)^{0.5}\left(\frac{L_B}{L_B + L_S}\right)^{0.3} \quad (4)$$

Table I shows some methods applicable to measure the amount of CO_2 absorbed from gas to liquid phase.

Table I. Absorbed CO_2 measurement method.

Inlet Fluid	Analysis Method	Reference
Liquid: Water + 30wt% DEA solution Gas: CO_2 / N_2	Titration of the output liquid phase is used to measure the absorbed CO_2.	[18]
Liquid: Pure water Gas: CO_2	Titration for the measurement of the absorbed CO_2	[3]
Liquid: MEA aqueous solution Gas: CO_2	An online assessment of the bubbles' volume to determine mass transfer coefficients	[19]
Liquid: NaOH aqueous solution Gas: CO_2 / N_2	Titrating the concentration of the liquid output to determine the amount of CO_2 absorbed	[20]
Liquid: NaOH aqueous solution Gas: CO_2 / N_2	Measuring the length of the slug to calculate the transferred CO_2	[21]
Liquid: NaOH aqueous solution Gas: CO_2 / N_2	Measuring the length of the slug to calculate the transferred CO_2	[22]
Liquid: 0.3M $KHCO_3$/ 0.3M K_2CO_3 aqueous solution Gas: CO_2 / N_2	Titrating the concentration of the liquid output to determine the amount of CO_2 absorbed	[23]
Liquid: Alkaline solution Gas: CO_2	Measurement of CO_2 absorption using the pH-LIFT method	[24]
Liquid: MEA-ethylene glycol aqueous solution Gas: CO_2 / N_2	An online assessment of the bubbles' volume to determine mass transfer coefficients	[25]

The titration method is suitable for measuring the concentration of CO_2 that is absorbed from the gas bubbles into water in the microchannel reactor. The method for determining the amount of physically absorbed CO_2 was to add the liquid sample from the sample collector to an excess NaOH solution and titrate with HCl solution. The first and second endpoint indicators were phenolphthalein and methyl orange, respectively. A comparable study was performed on the input water to serve as a blank titration [3, 20, 23]. Then, the mass transfer rate can be evaluated for slug flow with different dimensions.

A flow pattern map is a graphical representation used to identify the different flow regimes under varying operational conditions, such as flow rates and channel dimensions. It helps to categorize flow patterns such as slug flow, bubbly flow, annular flow, and churn flow, based on parameters like gas and liquid superficial velocities, flow rates, pressure, and fluid properties. This flow pattern map is a critical tool in designing and optimizing microchannel reactors for specific applications where mass transfer and reaction kinetics depend heavily on the type of flow regime present. Table II summarizes the flow pattern maps collection from previous related studies and experiments.

Table II. Summary of flow pattern map.

Microchannel Shape & Dimension	Feed	Superficial Velocities (m/s)	Flow Pattern	Reference
Rectangular **Width:** 9mm **Height:** 0.42mm	**Gas:** Nitrogen /air **Liquid:** Distilled water	**Gas:** 0.1-60 **Liquid:** 0.01-2	•Annular flow • Jet flow • Bubble flow • Stratified flow • Slug flow • Churn flow	[11]
Rectangular **Width:** 10mm **Height:** 0.3mm	**Gas:** Nitrogen /air **Liquid:** Distilled water	**Gas:** 0.1-60 **Liquid:** 0.01-2	• Churn flow • Stratified flow • Annular flow • Bubble flow • Pulsating flow	
Y-type Rectangular **Width:** 0.5mm **Height:** 1mm	**Gas:** CO_2 **Liquid:** water	**Gas:** 0.01-70 **Liquid:** 0.001-1	• Churn flow • Slug flow • Annular flow • Slug-annular flow • Bubbly flow	[26]
Y-type square **Width:** 0.4mm **Height:** 0.4mm		**Gas:** 0.01-40 **Liquid:** 0.001-1		
Y-type square **Width:** 0.2mm **Height:** 0.2mm		**Gas:** 0.01-10 **Liquid:** 0.001-1		
Circular **Diameter:** 1.097mm	**Gas:** CO_2 **Liquid:** water	**Gas:** 0.7-15 **Liquid:** 0.009-1	• Slug flow • Churn flow • Slug-annular flow	[3]

Microchannel Shape & Dimension	Feed	Superficial Velocities (m/s)	Flow Pattern	Reference
Circular **Diameter:** 1.097mm	**Gas:** CO_2 **Liquid:** water	**Gas:** 0.01-20 **Liquid:** 0.01-1	• Slug flow • Bubbly flow • Slug-annular flow • Annular flow • Churn flow	[6]
Circular **Diameter:** 100 µm	**Gas:** Air **Liquid:** water	**Gas:** 0.0707-192.232 **Liquid:** 0.0101-2.209	• Slug flow • Bubbly flow • Ring flow • Annular flow	[4]
Circular **Diameter:** 100 µm	**Gas:** Air **Liquid:** water	**Gas:** 0.0021-72.859 **Liquid:** 0.0020-3.498		
Circular **Diameter:** 100 µm	**Gas:** Air **Liquid:** water	**Gas:** 0.081-24.214 **Liquid:** 0.0020-2.527		

III. METHODOLOGY

A. Experimental Setup

The experimental setup in Fig. 2 consists of microfluidic feeding system and monitoring system. The water feeding system indicated by a syringe pump, a circular microchannel with a diameter of 700 µm. The gas (CO_2) feeding system supplied from CO_2 tank and the flow is controlled using a mass flow controller before it flowed through a 350 µm circular microchannel. The inlet CO_2 gas and inlet water flowed into main 700 µm microchannel with 45cm length through a T-junction. The flow rate of CO_2 gas and water were in the ranges of 0.4 – 0.85 ml/min and 0.2 – 0.8 ml/min respectively. A microscope equipped with a high-speed camera was used to observe the flow inside the main microchannel. It is connected to a computer and the flow can be viewed in "ToupView" software. The software processes the image taken from the camera to be viewed at the computer display and for measurement and recording purpose. It was calibrated using a stage micrometer to ensure accurate measurement of the captured images. Additionally, the titration method was used to measure the amount of CO_2 absorbed into water as shown in Fig. 3.

B. Experimental Procedure

The CO_2 and water were injected into the respective inlet microchannel at an ambient temperature of 25°C and pressure of 1atm. The flow rate of CO_2 was adjusted using the mass flow controller while the flow rate of water was adjusted using the syringe pump. The digital camera was utilized to capture the images of the flow pattern inside the microchannel. The procedures were repeated by manipulating the flow rates of CO_2 and water. From the captured image, the type of flow pattern was determined and recorded. Then, the gas bubble and liquid slug dimensions were measured accordingly. Then, a flow pattern map with variations of flow regimes at certain superficial velocities was plotted accordingly.

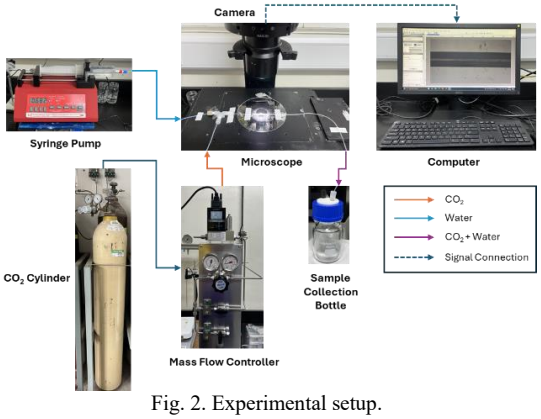

Fig. 2. Experimental setup.

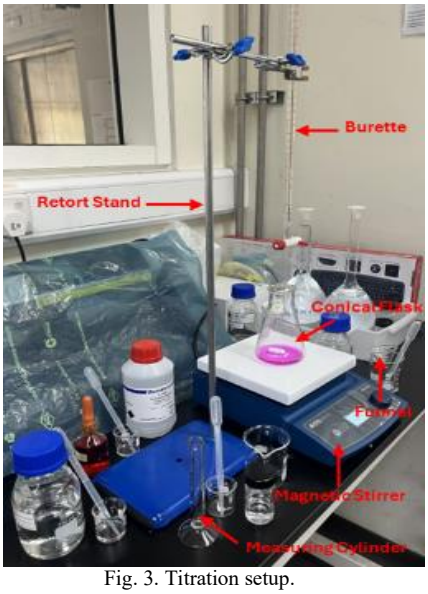

Fig. 3. Titration setup.

For titration, the sample (10 ml) from sample collection bottle was added into a clean titration flask with an excess of 0.05 M NaOH solution (5 ml). Then a drop of phenolphthalein indicator was added to the solution. It turned into a pink colour which indicated an alkaline medium. Next 0.1 M of HCl was filled into a burette. Titration started by adding the acid slowly into the solution while gently swirling the flask. The first endpoint was obtained when the phenolphthalein indicator turned into colourless. Then, a drop of methyl orange indicator was added. Then, acid was added slowly until the solution turned from yellow to red indicated the second endpoint. The difference in acid consumed from both steps corresponded to the amount of absorbed CO_2. The concentration of absorbed CO_2 was determined based on Eqs. (5) to (11) accordingly.

C. Absorbed CO_2 Determination Method

Table III. Titration guidance.

Endpoint	Measured Value	Purpose
1st endpoint – Phenolphthalein Indicator	Volume of HCl used (V_1)	Reflect the neutralization of excess NaOH that has not reacted with CO_2.
2nd endpoint – Methyl orange indicator	Volume of HCl used (V_2)	Reflect the neutralization of all amounts of NaOH (unreacted and reacted with CO_2)

The reaction between absorbed CO_2 in water and excess NaOH:

$$CO_2 + 2NaOH \rightarrow Na_2CO_3 + H_2O \quad (5)$$

Reaction between NaOH (excess that has not reacted with CO_2) and HCl:

$$HCl + NaOH \rightarrow NaCl + H_2O \quad (6)$$

Moles of NaOH that reacted with CO_2 completely:

$$V_{HCl} = V_2 - V_1 \quad (7)$$

$$n_{HCl} = V_{HCl} \times C_{HCl} \quad (8)$$

$$n_{NaOH,reacted} = n_{HCl} \quad (9)$$

Concentration of absorbed CO_2 in water:

$$n_{CO_2} = \frac{n_{NaOH,reacted}}{2} \quad (10)$$

$$C_{CO_2} = \frac{n_{CO_2}}{V_{sample}} \quad (11)$$

IV. RESULTS AND DISCUSSION

A. Dimension Measurement and Flow Pattern Map

There were three different flow patterns observed which were slug flow, bubble flow and slug-bubbly flow. "Set No." in Table IV indicates the respective pair of CO_2 and water flow rates. The flow dimensions included bubble length (L_B), slug length (L_S), liquid film length (L_F) and bubble diameter (d_B). However, bubbly-slug dimension was not measured because it was an alternate of slug and bubble flow throughout the experiment.

When the CO_2 flow rate was constant at 0.4 ml/min while the water flowrate increased from 0.2 to 0.35 ml/min, slug flow was observed with decreasing gas bubble length and increasing liquid slug length. However, at 0.5 ml/min of water, a bubbly-slug flow was formed. This pair of CO_2 and water flowrate indicates the boundary line which is the transition between bubble flow and slug flow. Then, when the water flow rate further increased to 0.65 and 0.8 ml/min at constant CO_2 flow rate, bubble flow was formed with decreasing bubble length. These results show that the gas-to-liquid ratio affects the type of flow regimes along with the size of gas bubble and liquid slug. Similar trend was observed when the CO_2 flow rate increased from 0.4 to 0.85 ml/min. Slug flow formed at high gas-to-liquid ratio (>1) while bubble flow formed at low gas-to-liquid ratio (<1).

Table IV. Dimension of gas bubble and liquid slug for each flow pattern.

Set No.	Q_g (ml/min)	Q_l (ml/min)	G:L ratio	Flow Pattern	L_B (µm)	L_F (µm)	L_S (µm)	d_B (µm)
1	0.40	0.20	2.00	Slug	1645.85	1310.48	728.25	652.51
2		0.35	1.14	Slug	840.06	557.87	850.09	650.70
3		0.50	0.80	Bubbly-Slug	-	-	-	-
4		0.65	0.62	Bubble	485.56	-	1156.29	646.14
5		0.80	0.50	Bubble	386.03	-	1522.87	501.95
6	0.55	0.20	2.75	Slug	2060.21	1767.25	630.62	665.30
7		0.35	1.57	Slug	1358.94	1041.30	889.84	658.44
8		0.50	1.10	Slug	876.12	575.86	833.68	651.62
9		0.65	0.85	Bubble	657.59	-	988.36	654.84
10		0.80	0.69	Bubble	478.68	-	1141.97	636.61
11	0.70	0.20	3.50	Slug	2440.81	2147.11	589.65	670.77
12		0.35	2.00	Slug	1568.60	1269.42	762.49	648.86
13		0.50	1.40	Slug	1266.73	949.58	926.05	657.55
14		0.65	1.08	Slug	777.04	465.44	877.48	659.38
15		0.80	0.88	Bubbly-Slug	-	-	-	-
16	0.85	0.20	4.25	Slug	3122.74	2817.35	577.03	664.62
17		0.35	2.43	Slug	1734.62	1389.69	689.24	670.99
18		0.50	1.70	Slug	1427.32	1078.94	832.29	651.82
19		0.65	1.31	Slug	983.33	629.25	730.53	652.98
20		0.80	1.06	Slug	771.62	444.94	861.50	648.41

In terms of length, the gas bubble length decreases with gas-to-liquid ratio, but the liquid slug length increases [6, 9, 12]. For example, at constant CO_2 flow rate of 0.85 ml/min, slug flow was observed for all water flow rates. When the water flow rate increased from 0.2 to 0.8 ml/min, the bubble length decreased from 3122.74 to 771.62 µm while the liquid slug increased from 577.03 to 861.50 µm. In conclusion, higher gas-to-liquid ratio produces a longer slug flow consists of gas bubbles that are closer to each other. On the other hand, as the gas-to-liquid ratio decreases, shorter slug flow is formed consists of gas bubbles that are further to each other. In Fig. 4, the change in length for gas bubble and liquid can be observed where a longer gas bubble has a shorter liquid slug. The change of gas bubble and liquid slug are in opposite direction.

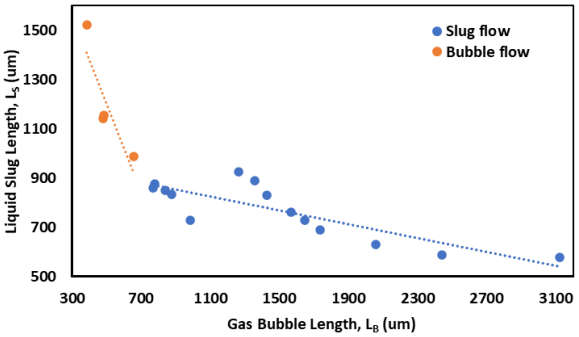

Fig. 4. Gas bubble length vs liquid slug length.

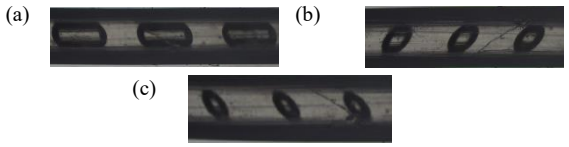

Fig. 5. Image of (a) Slug flow, (b) Spherical bubble flow and (c) Ellipsoidal bubble flow.

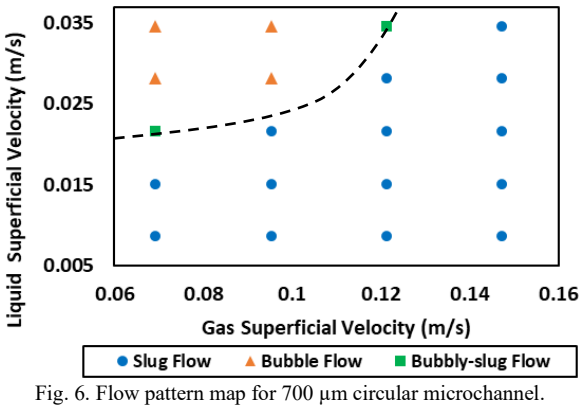

Fig. 6. Flow pattern map for 700 µm circular microchannel.

From the types of flow regime observed, a flow pattern map was developed in Fig. 6. Most of the flow inside the circular microchannel was slug flow as shown in Fig. 5(a). The slug flow is dominant at high CO_2 superficial velocity, J_g and low water superficial velocity, J_l which gives higher gas-to-liquid ratio. As the gas superficial velocity increases, CO_2 momentum causes the development of elongated gas slugs to become more dominant. On the other hand, bubble flow as shown in Fig. 5 (b) and Fig. 5(c) tends to form at low J_g and high J_l which gives lower gas-to-liquid ratio. Higher water flow causes the gas phase to break up into smaller bubbles, resulting in a more dispersed regime. The higher liquid velocity enhances bubble fragmentation due to increased shear forces. The increasing shear force during gas bubble formation results in shorter gas bubble length [2]. Additionally, a small region of bubbly-slug flow is observed between slug flow and bubble flow. This implies a transition between those two main flow regimes. The dotted line across the bubbly-slug region used to indicate the boundary line between two flow regimes in the flow pattern map. From this new flow pattern map, any CO_2 application using circular microchannel can refer to this flow pattern map so that the optimum range can be determined to obtain the desired flow regime.

From Fig. 7, it shows an increasing trend of Taylor bubble length (CO_2) with gas-to-liquid superficial velocity ratio. On the other hand, the liquid slug length (water) decreases at higher gas-to-liquid superficial velocity ratio as shown in Fig. 8. The increase in J_g at constant J_l resulted in longer bubbles and shorter liquid slugs [3]. The higher gas-to-liquid superficial velocity ratio indicates the increment in gas superficial velocity which contributes to the increasing of shear stress and decreasing of viscosity [9].

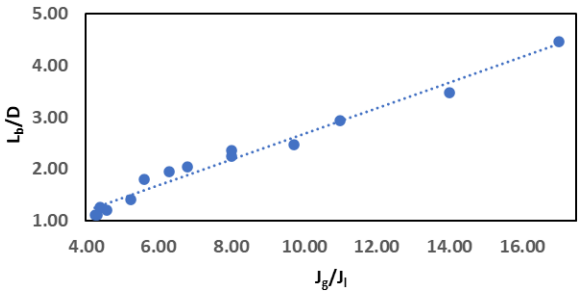

Fig. 7. Effect of gas-to-liquid ratio on gas bubble length.

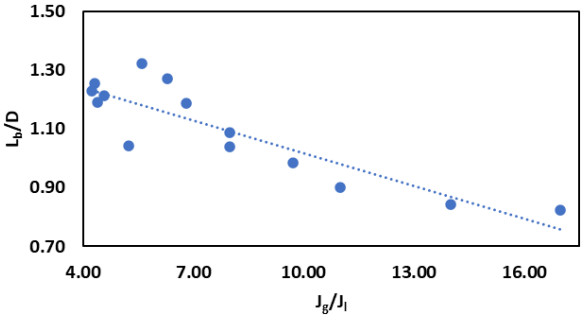

Fig. 8. Effect of gas-to-liquid ratio on liquid slug length.

B. Interfacial Area

The surface area of single gas bubble was determined by using specific surface area formula based on the gas bubble's shape. Then, the total number of gas bubbles across the microchannel length was estimated by using the domain length (L_d) or unit cell with assumptions of constant and stable domain length. However, in actual case the gas bubble gradually decreases as it flows through the microchannel [12].

For slug flow, the gas bubble formed inside microchannel showed a cylindrical shape. So, the surface area of single gas bubble was calculated by using the surface area of a cylinder with two hemispheres as the head and tail of the gas bubble as shown in Eq. (12) [16]. For bubble flow, there were two different shapes observed. The gas bubble that was closed to a sphere was calculated using spherical surface area as described in Eq. (13). The gas bubble that looked like a sphere but slightly compressed was calculated using ellipsoidal surface area based on Knud Thomsen's approximation, where P ≈ 1.6 as described in Eq. (14).

$$A_{slug} = 2\pi\left(\frac{d_B}{2}\right)L_T + 4\pi\left(\frac{d_B}{2}\right)^2 \quad (12)$$

$$A_{bubble,spherical} = 4\pi\left(\frac{d_B}{2}\right)^2 \quad (13)$$

$$A_{bubble,ellipsoidal} = 4\pi\left(\frac{2\left[\left(\frac{L_B}{2}\right)\left(\frac{d_B}{2}\right)\right]^P + \left(\frac{d_B}{2}\right)^{2P}}{3}\right)^{\frac{1}{P}} \quad (14)$$

The total number of gas bubbles in the microchannel was calculated based on the domain length as illustrated by dashed line in Fig. 9, Fig. 10 and Fig. 11. So, the number of gas bubbles inside the entire microchannel was estimated by dividing the total microchannel length with the domain length, L_d as described in Eq. (15).

$$Total\ number\ of\ gas\ bubbles = \frac{Microchannel\ Length}{Domain\ Length} = \frac{L_T}{L_d} \quad (15)$$

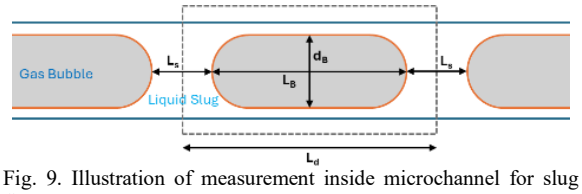

Fig. 9. Illustration of measurement inside microchannel for slug flow.

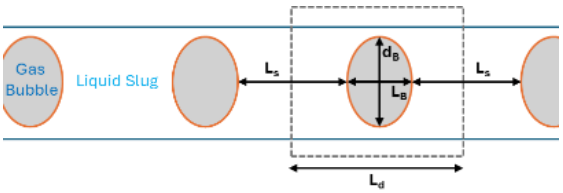

Fig. 10. Illustration of measurement inside microchannel for bubble flow (ellipsoidal).

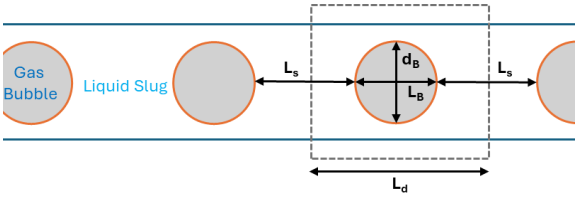

Fig. 11. Illustration of measurement inside microchannel for bubble flow (spherical).

Different flow dimensions give different number of total gas bubbles. The flow with longer gas bubble consists of larger individual surface area but the total number of gas bubbles produced is lower compared to the flow with shorter gas bubbles as shown in Fig. 12. However, the flow with longer gas bubble has higher total interfacial area after considering the total surface area from total number of gas bubbles as shown in Fig. 13. This is because the flow with shorter gas bubble has a greater number of bubbles, but the difference is not very significant to achieve higher total surface area compared to the flow with longer gas bubble. The increase in interfacial area with bubble length can be attributed to the cylindrical geometry of Taylor bubbles, which adds both axial and radial surface area. Despite a reduction in bubble count, their individual surface area compensates, maintaining higher cumulative contact area.

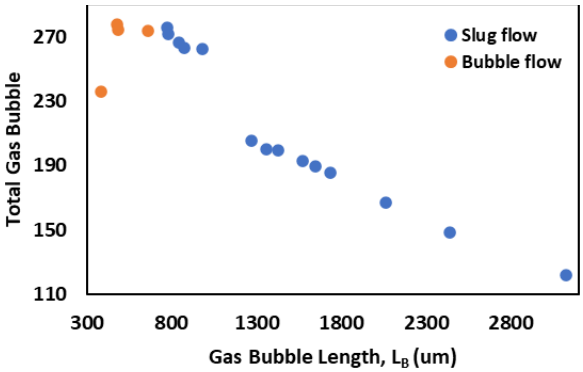

Fig. 12. Gas bubble length vs total number of gas bubbles.

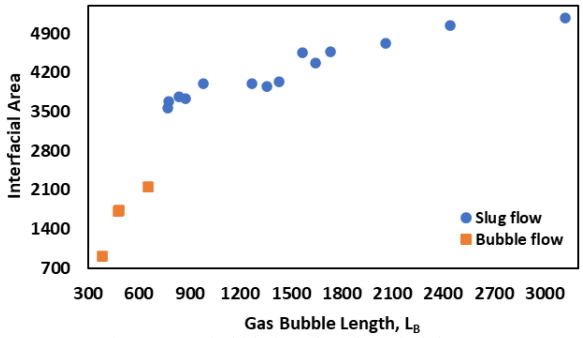

Fig. 13. Gas bubble length vs interfacial area.

At a constant CO_2 flow rate, the interfacial area decreases with increment of water flow rate (lower gas-to-liquid ratio). This is due to the smaller size of gas bubble formed. However, at constant water flow rate, the interfacial area increases with CO_2 flow rate (higher gas-to-liquid ratio). This information is illustrated in Fig. 14. For example, in Set No. 1,6,11 and 16, the slug flow is formed at 0.2 ml/min of water and 0.4, 0.55, 0.7 and 0.85 ml/min of CO_2 respectively. The total interfacial area increases from 4375.57 to 5172.32 m^2/m^3. Same goes to other set of constant water flow rate because the contact area between the gas bubble and liquid phase including bubble velocity increases as the gas flow rate increases [12]. The significant increment in the interfacial area leads to better overall volumetric mass transfer coefficient [13].

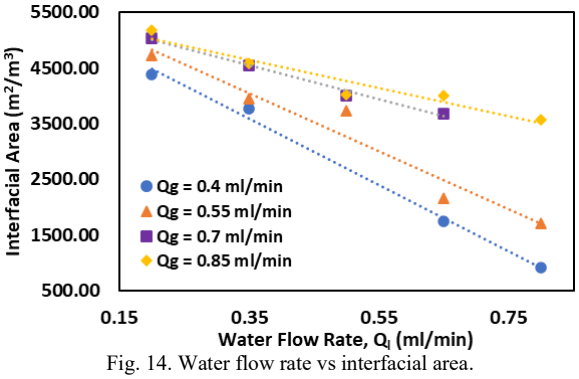

Fig. 14. Water flow rate vs interfacial area.

The titration data represents the mass transfer of CO_2 from the gas bubble into liquid phase in the microchannel. The initial concentration of CO_2 was measured from a blank sample (distilled water) while the final concentration of CO_2 was measured from the collected sample after distilled water and CO_2 passed through the microchannel. Higher total interfacial area allows more CO_2 to be absorbed from gas bubble into water within the same microchannel length. The titration results show the amount of HCl used to neutralize the sample with excess NaOH. Then concentration of absorbed CO_2 was calculated accordingly.

The size of gas bubbles is increasing from bubble flow to slug flow. The total interfacial area is increasing at constant microchannel volume. So, the concentration of the absorbed CO_2 increases due to the increment of mass transfer area between two phases as shown in Fig. 15. This trend indicates that the interfacial area affects mass transfer in the microchannel reactor for multiphase flow system. It also proves that the mass transfer of CO_2 occurred on the whole surface area of the Taylor bubble.

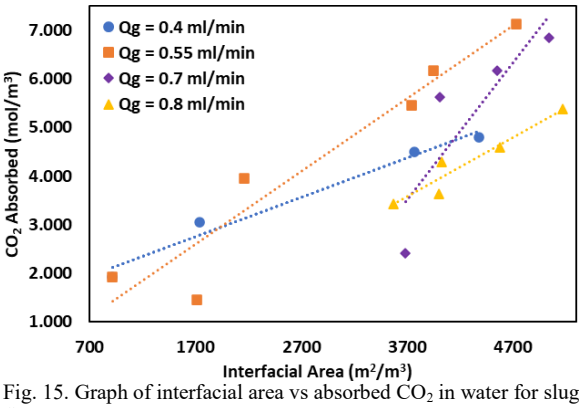

Fig. 15. Graph of interfacial area vs absorbed CO_2 in water for slug flow.

C. Rate of Mass Transfer

According to the mass transfer rate concept in Eq. (16), the mass transfer rate is proportional to the surface area of mass transfer and concentration difference. The slug flow provides an effective mass transfer because the liquid slug's circulation flow continually renews the liquid interface, allowing for fast mass transfer between two phases [15]. Specifically for slug flow, the liquid side volumetric mass transfer coefficient was calculated using Eq. (4) , where d_h is the hydraulic diameter, D is liquid phase diffusivity, u_B is velocity of Taylor bubble, L_B is bubble length and L_S is slug length.

$$\dot{m} = k_L A \Delta C \tag{16}$$

$$\dot{m} = k_L a V \Delta C \tag{17}$$

The mass transfer rate of slug flow is analyzed to study their correlation with interfacial area. More CO_2 is absorbed into the water when the contact area is larger from the titration result. So, the higher interfacial area led to better mass transfer rate. The mass transfer took place not just on the bubble caps, but also on the thin film between the bubble and the channel wall [27]. Thus, longer slug flow has better mass transfer because of larger mass transfer area between gas and liquid phase. The graph shown in Fig. 16 illustrates the relationship between interfacial area and mass transfer rate for slug flow. As expected, the interfacial area and mass transfer rate have a positive relationship, which means that as the interfacial area grows, so does the mass transfer rate. This tendency aligns with the fundamental mass transfer principles, where a larger interfacial area promotes gas-liquid interaction and enables more CO_2 absorption from gas into water.

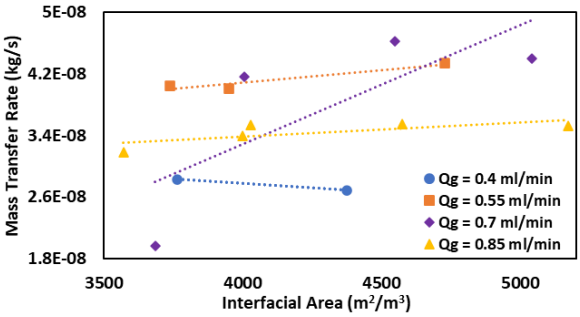

Fig. 16. Graph of interfacial area vs mass transfer rate for slug flow.

V. CONCLUSION

In this study, the flow pattern hydrodynamics has been investigated inside a microchannel. A 700 µm circular microchannel was used and three flow regimes were observed which were slug flow, bubble flow and bubbly-slug flow. Then, the flow pattern map of CO_2 and water in a circular microchannel was plotted based on the superficial velocities of CO_2 and water. The desired slug flow is favourable at high gas superficial velocity which gives higher gas-to-liquid ratio. The slug flow recorded higher interfacial area compared to the bubble flow. Factors that affected the interfacial area were the types of flow patterns and flow dimensions. At high gas-to-liquid ratio, longer gas bubble and shorter liquid slug are formed. At the same time, the total number of gas bubbles decreased. The slug flow with longer gas bubbles has higher total interfacial area due to insignificant difference in the gas bubbles number. In the end, the higher total interfacial area contributes to the higher mass transfer rate. So, it can be concluded that the longer slug flow provides the highest mass transfer rate of CO_2 in microchannels.

ACKNOWLEDGEMENT

In the name of Allah, the Most Gracious and the Most Merciful. Alhamdulillah, all praises to Allah for His blessing. I would like to thank the Chemical Engineering Department, Universiti Teknologi PETRONAS for providing the opportunity and funding support to conduct this research.

REFERENCES

[1] H. Ritchie, P. Rosado and M. Roser, "CO_2 and Greenhouse Gas Emissions." Our World in Data. [Available online on September 2024] https://ourworldindata.org/co2-and-greenhouse-gas-emissions.

[2] Y. Chen, Y. Yang, G. Wang, F. Huo and C. Li, "Revealing The Effect of Water on The CO_2-Ionic Liquid System in Microchannels: Physical Properties, Hydrodynamics and Mass Transfer Behavior," *Chem. Eng. Sci.,* vol. 301, pp. 120617, 2025.

[3] J. Yue, G. Chen, Q. Yuan, L. Luo and Y. Gonthier, "Hydrodynamics and Mass Transfer Characteristics in Gas–Liquid Flow Through A Rectangular Microchannel," *Chem. Eng. Sci.,* vol. 62, no. 7, pp. 2096-2108, 2007.

[4] A. Sur and D. Liu, "Adiabatic Air–water Two-phase Flow in Circular Microchannels," *Int. J. Therm. Sci.,* vol. 53, pp. 18-34, 2012.

[5] P. Rosa, T. G. Karayiannis and M. W. Collins, "Single-phase Heat Transfer in Microchannels: The Importance of Scaling Effects," *Appl. Therm. Eng.,* vol. 29, no. 17-18, pp. 3447-3468, 2009.

[6] M. Akbari, M. Rahimi and M. Faryadi, "Gas–liquid Flow Mass Transfer in A T-Shape Microreactor Stimulated with 1.7 MHz Ultrasound Aaves," *Chin. J. Chem. Eng.,* vol. 25, no. 9, pp. 1143-1152, 2017.

[7] G. R, V. Thangarasu, M. A. Vinayakaselvi and A. Ramanathan, "A Critical Review of Recent Advancements in Continuous Flow Reactors and Prominent Integrated Microreactors for Biodiesel Production," *Renew. and Sustain. Ener. Rev.,* vol. 154, pp. 111869, 2022.

[8] L. Yang, K. Loubière, N. Dietrich, C. Le Men, C. Gourdon and G. Hébrard, "Local Investigations on The Gas-Liquid Mass Transfer Around Taylor Bubbles Flowing in A Meandering Millimetric Square Channel," *Chem. Eng. Sci.* vol. 165, pp. 192-203, 2017.

[9] Q. Li *et al.*, "Experimental Study of Taylor Bubble Flow in Non-Newtonian Liquid in A Rectangular Microchannel," *Chem. Eng. Sci.,* vol. 252, pp. 117509, 2022.

[10] R. Yun and Y. Kim, "Flow Regimes For Horizontal Two-phase Flow Of CO_2 in A Heated Narrow Rectangular Channel," *Int. J. Multiphase Flow,* vol. 30, no. 10, pp. 1259-1270, 2004.

[11] E. A. Chinnov, F. V. Ron'shin and O. A. Kabov, "Two-phase Flow Patterns in Short Horizontal Rectangular Microchannels," *Int. J. Multiphase Flow,* vol. 80, pp. 57-68, 2016.

[12] Y. Yin, C. Zhu, R. Guo, T. Fu and Y. Ma, "Gas-liquid Two-phase Flow in A Square Microchannel with Chemical Mass Transfer: Flow Pattern, Void Fraction and Frictional Pressure Drop," *Int. J. Heat and Mass Transf.,* vol. 127, pp. 484-496, 2018.

[13] M. Sattari-Najafabadi, M. Nasr Esfahany, Z. Wu and B. Sunden, "Mass Transfer Between Phases in Microchannels: A Review," *Chem. Eng. and Process. - Process Intensif.,* vol. 127, pp. 213-237, 2018.

[14] E. S. P. D. Ortiz, *Mass Transfer Coefficients*, Begellhouse eBooks, 2008.

[15] K. Miyabayashi, O. Tonomura, K. I. Sotowa and S. Hasebe, "Slug Length Estimation for Gas-liquid Slug Flow in T-shaped Microdevices with Liquid Film," *IFAC-PapersOnLine,* vol. 55, no. 7, pp. 210–215, 2022.

[16] J. Yue, L. Luo, Y. Gonthier, G. Chen and Q. Yuan, "An Experimental Study of Air–water Taylor Flow and Mass Transfer Inside Square Microchannels," *Chem. Eng. Sci.,* vol. 64, no. 16, pp. 3697-3708, 2009.

[17] Y. Li and H. Lv, "Numerical Simulation of Mass Transfer of Slug Flow in Microchannel," *Chem. Eng. Trans.*, vol. 65, pp. 325-330,2018.

[18] C. Yao, K. Zhu, Y. Liu, H. Liu, F. Jiao and G. Chen, "Intensified CO_2 Absorption in A Microchannel Reactor Under Elevated Pressures," *Chem. Eng. J.,* vol. 319, pp. 179-190, 2017.

[19] C. Zhu, C. Li, X. Gao, Y. Ma and D. Liu, "Taylor Flow and Mass Transfer of CO_2 Chemical Absorption into MEA Aqueous Solutions in A T-Junction Microchannel," *Int. J. Heat and Mass Transf.,* vol. 73, pp. 492-499, 2014.

[20] H. Su, S. Wang, H. Niu, L. Pan, A. Wang and Y. Hu, "Mass Transfer Characteristics of H_2S Absorption from Gaseous Mixture into Methyldiethanolamine Solution in A T-Junction Microchannel," *Separ. and Purif. Technol.,* vol. 72, no. 3, pp. 326-334, 2010.

[21] J. Tan, Y. C. Lu, J. H. Xu and G. S. Luo, "Mass Transfer Performance of Gas–liquid Segmented Flow in Microchannels," *Chem. Eng. J.,* vol. 181-182, pp. 229-235, 2012.

[22] J. Tan, Y. C. Lu, J. H. Xu and G. S. Luo, "Mass transfer Characteristic in The Formation Stage of Gas–liquid Segmented Flow in Microchannel," *Chem. Eng. J.,* vol. 185-186, pp. 314-320, 2012.

[23] P. Sobieszuk, R. Pohorecki, P. Cygański and J. Grzelka, "Determination of The Interfacial Area and Mass Transfer Coefficients in The Taylor Gas–Liquid Flow in A Microchannel," *Chem. Eng. Sci.,* vol. 66, no. 23, pp. 6048-6056, 2011.

[24] S. Kuhn and K. F. Jensen, "A pH-Sensitive Laser-Induced Fluorescence Technique to Monitor Mass Transfer in Multiphase Flows in Microfluidic Devices," *Industr. & Eng. Chem. Res.,* vol. 51, no. 26, pp. 8999-9006, 2012.

[25] L. Yang, J. Tan, K. Wang and G. Luo, "Mass Transfer Characteristics of Bubbly Flow in Microchannels," *Chem. Eng. Sci.,* vol. 109, pp. 306-314, 2014.

[26] J. Yue, L. Luo, Y. Gonthier, G. Chen and Q. Yuan, "An Experimental Investigation of Gas–liquid Two-phase Flow in Single Microchannel Contactors," *Chem. Eng. Sci.,* vol. 63, no. 16, pp. 4189-4202, 2008.

[27] W. Huang, X. Ren, L. Xiao, K. Zheng, X. H. Ge and X. Wang, "Sizing-up Effect on The Flow Pattern and Mass Transfer of Gas–liquid-liquid Three-phase Flow in Microchannels," *Exp. Ther. and Fluid Sci.,* vol. 159, pp. 111299, 2024.